JACS
JOURNAL OF THE AMERICAN CHEMICAL SOCIETY
Article
pubs.acs.org/JACS

Tetrathiafulvalene Hetero Radical Cation Dimerization in a Redox-Active [2]Catenane

Cheng Wang,[†] Scott M. Dyar,[†,‡] Dennis Cao,[†,§] Albert C. Fahrenbach,[†,§] Noah Horwitz,[†,‡] Michael T. Colvin,[†,‡] Raanan Carmieli,[†,‡] Charlotte L. Stern,[†] Sanjeev K. Dey,[†] Michael R. Wasielewski,*[,†,‡] and J. Fraser Stoddart*[,†,§]

[†]Department of Chemistry, Northwestern University, 2145 Sheridan Road, Evanston, Illinois 60208, United States

[‡]Argonne-Northwestern Solar Energy Research (ANSER) Center, Northwestern University, 2145 Sheridan Road, Evanston, Illinois 60208, United States

[§]NanoCentury KAIST Institute and Graduate School of EEWS (WCU), Korea Advanced Institute of Science and Technology (KAIST), 37-1 Guseong Dong, Yuseong Gu, Daejeon 305-701, Republic of Korea

Supporting Information

ABSTRACT: The electronic properties of tetrathiafulvalene (TTF) can be tuned by attaching electron-donating or electron-withdrawing substituents. An electron-rich macrocyclic polyether containing two TTF units of different constitutions, namely 4,4′-bis(hydroxymethyl)-tetrathiafulvalene (OTTFO) and 4,4′-bisthiotetrathiafulvalene (STTFS), has been synthesized. On two-electron oxidation, a hetero radical dimer is formed between $OTTFO^{\bullet+}$ and $STTFS^{\bullet+}$. The redox behavior of the macrocyclic polyether has been investigated by electrochemical techniques and UV−vis and electron paramagnetic resonance (EPR) spectroscopies. The [2]catenane in which the macrocyclic polyether is mechanically interlocked with the cyclobis(paraquat-*p*-phenylene) ($CBPQT^{4+}$) ring has also been prepared using template-directed protocols. In the case of the [2]catenane, the formation of the TTF hetero radical dimer is prevented sterically by the $CBPQT^{4+}$ ring. After a one-electron oxidation, a 70:30 ratio of $OTTFO^{\bullet+}$ to $STTFS^{\bullet+}$ is present at equilibrium, and, as a result, two translational isomers of the [2]catenane associated with these electronically different isomeric states transpire. EPR titration spectroscopy and simulations reveal that the radical states of the two constitutionally different TTF units in the [2]catenane still experience long-range electronic intramolecular coupling interactions, despite the presence of the $CBPQT^{4+}$ ring, when one or both of them are oxidized to the radical cationic state. These findings in the case of both the free macrocyclic polyether and the [2]catenane have led to a deeper fundamental understanding of the mechanism of radical cation dimer formation between constitutionally different TTF units.

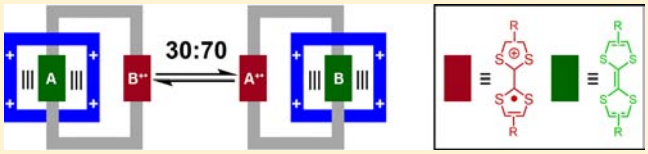

INTRODUCTION

The use[1] of conducting polymers in organic electronics devices, such as organic light-emitting diodes (OLEDs)[2] and organic photovoltaic cells (OPVCs),[3] has been making remarkable inroads into the commercial world in recent times. The interactions[4] of radical cations within these conducting polymers are vital to the mechanisms of their operation in these devices. Numerous studies have been conducted[5] on radical cation dimerization in π-conjugated oligomers during the past few decades with the specific aim of unraveling the nature of the charge-transport phenomena that occur in doped conducting polymers. For example, the π-stacking interactions of oligothiophene radical cations have been used[6] as a model for positively doped polythiophenes. Investigations into the mechanism of the interaction between radical cations not only deepen the understanding of the chemistry of this particular organic building block but also provide fundamental information necessary for the construction of organic electronic devices.

Derivatives of tetrathiafulvalene (TTF), well known for their π-electron-donating abilities, have received[7,8] a tremendous amount of attention over the past 40 years, partly because of their two reversible oxidation processes. This property has led to broad applications in host−guest chemistry,[9] mechanostereochemistry,[10] molecular electronics,[11] and materials science.[12] As a consequence of their stability, radical cation dimers have also attracted[13] a lot of interest. A one-electron oxidation of TTF generates the radical cation monomer ($TTF^{\bullet+}$), which can associate spontaneously under appropriate conditions to form the radical cation dimer $(TTF^{\bullet+})_2$ as a consequence of favorable radical−radical[13e] interactions, typically at high concentrations and low temperatures in solution.[13a−d] These favorable interactions between $TTF^{\bullet+}$ radical cations lead to the continuous π-stacks which are observed[14] in the solid state. It is very difficult, however, to form $(TTF^{\bullet+})_2$ dimers in relatively dilute solutions at room temperature as a consequence of their

Received: August 1, 2012
Published: November 9, 2012

dx.doi.org/10.1021/ja307577t | J. Am. Chem. Soc. 2012, 134, 19136−19145

Scheme 1. Synthesis of Macrocyclic Polyether 1, Obtained from 4 and 5 in High Dilution in the Presence of CsOH, Together with the Structures of OTTFO-TEG (2) and STTFS-TEG (3)

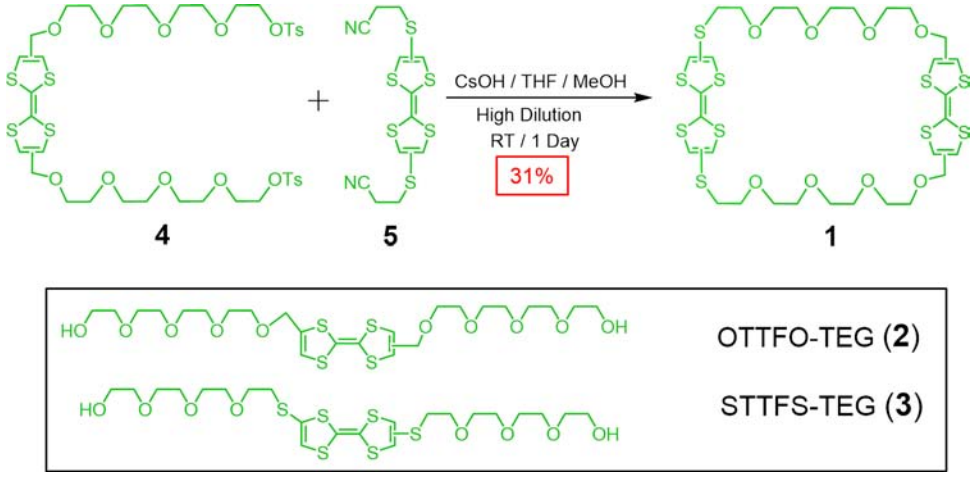

low stability. Several strategies have been employed to stabilize $(TTF^{\bullet+})_2$ dimers, namely, (i) covalent attachment[15] of the TTF units in a preorganized geometry to facilitate the formation of the dimers, (ii) using appropriate host molecules[16] such as molecular cages or rigid macrocyclic receptors, i.e., cucurbit[8]-uril or cyclodextrin, and (iii) stabilization by means[17] of mechanical bonds. Although TTF radical cation dimers that form between identical derivatives of TTF are widely known, TTF radical cation heterodimers, i.e., those composed of two structurally and electronically different TTF units, have not been investigated to the same extent.

Herein, we describe (i) the synthesis of a macrocyclic polyether incorporating two different TTF units, (ii) the formation of TTF radical cation heterodimers in this macrocyclic polyether and the elucidation of its redox mechanism, as characterized by electrochemistry, UV−vis, and electron paramagnetic resonance (EPR) spectroscopies, (iii) the template-directed synthesis, characterization, and X-ray crystal structure of a donor−acceptor [2]catenane composed of this macrocyclic polyether, mechanically interlocked with the cyclobis(paraquat-*p*-phenylene) ($CBPQT^{4+}$) ring, and (iv) the mechanistic role these two TTF radical cations play within a mechanically interlocked molecule.

RESULTS AND DISCUSSION

Macrocycle 1. As a result of recent advances[7,18] in synthetic methodologies, a myriad of new TTF derivatives is available. Scheme 1 shows two structurally different TTF derivatives: 4,4′-bis((2-(2-(2-hydroxyethoxy)ethoxy)ethoxy)ethoxymethylene)tetrathiafulvalene[19] (OTTFO-TEG, **2**) and 4,4′(5′)-bis(2-(2′-(2″-(2‴-hydroxyethoxy)ethoxy)ethoxy)ethylthio)-tetrathiafulvalene[10e] (STTFS-TEG, **3**). Starting from compounds **4** and **5**,[20] the macrocyclic polyether **1** bearing both OTTFO and STTFS units can be synthesized in the presence of CsOH under high dilution conditions in 31% yield.

The oxidation potentials of TTF can be finely tuned by the covalent attachment of electron-donating or electron-withdrawing substituents to the 3 and 4 carbon atoms of the five-membered rings. Cyclic voltammetry (CV), performed in MeCN at room temperature, was used to investigate (Figure 1) the electrochemical behavior of **2** and **3**, along with that of the macrocyclic polyether **1**. The CV of **2** shows two redox processes at +400 and +750 mV, corresponding to two reversible one-electron oxidations, $\mathbf{2}\rightarrow\mathbf{2}^{\bullet+}$ and $\mathbf{2}^{\bullet+}\rightarrow\mathbf{2}^{2+}$, respectively. In the case of STTFS-TEG, because of the electron-withdrawing alkylthio groups,[21] both oxidation processes are observed at more positive potentials, +470 and +840 mV. When incorporated into the macrocyclic polyether **1**, however, the oxidation processes of the OTTFO and STTFS units appear at the same potentials. The CV of **1** reveals two two-electron redox processes, one at +370 mV and the other at +850 mV. The first oxidation potential of **1** is shifted negatively while the second oxidation is shifted positively with reference to both **2** and **3**, suggesting that a stable species—namely, a radical cation heterodimer $[OTTFO^{\bullet+}\cdots STTFS^{\bullet+}]$—is formed after the first two-electron oxidation process.

UV−vis spectroscopic experiments were carried out in support of the supposition that the hetero radical dimer $[OTTFO^{\bullet+}\cdots STTFS^{\bullet+}]$ is formed when **1** is oxidized. As a control, UV−vis spectroscopic titrations of the one-electron oxidizing agent $Fe(ClO_4)_3$ into solutions of both **2** and **3** in MeCN at room temperature were carried out. In the case of **2**, after the addition of 1 equiv of $Fe(ClO_4)_3$, characteristic absorption bands[17] for the $OTTFO^{\bullet+}$ radical cation unit with λ_{max} = 450 and 600 nm were detected (Figure 2a). After further addition of $Fe(ClO_4)_3$ up to 2 equiv, the peaks at 450 and 600

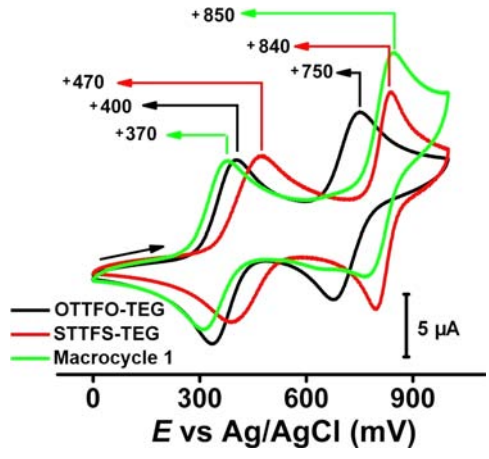

Figure 1. Cyclic voltammetry traces of OTTFO-TEG (**2**), STTFS-TEG (**3**), and the macrocycle **1**. All experiments were conducted in argon-purged MeCN (0.5 mM, 0.1 M $TBAPF_6$, 200 $mV{\cdot}s^{-1}$) at 298 K.

dx.doi.org/10.1021/ja307577t | J. Am. Chem. Soc. 2012, 134, 19136−19145

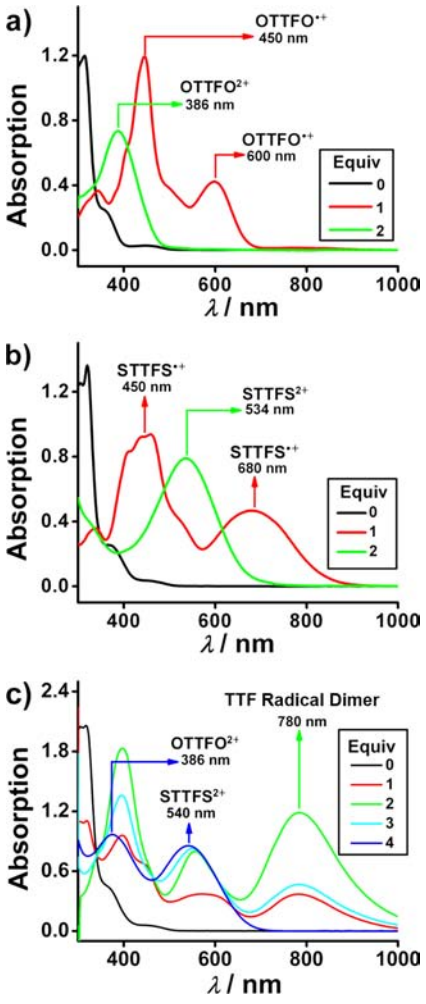

Figure 2. Absorption spectra (MeCN, 298 K) of a 1.0×10^{-4} M solution of (a) OTTFO-TEG (**2**), (b) STTFS-TEG (**3**), and (c) the macrocyclic polyether **1**, after the addition of different equivalents of $Fe(ClO_4)_3$.

nm disappeared, and a new absorption band emerged around 386 nm, which is assigned[17] (Figure 2a) to the $OTTFO^{2+}$ dication. When 1 equiv of $Fe(ClO_4)_3$ was added to **3** to generate $\mathbf{3}^{\bullet+}$, the absorption bands of the $STTFS^{\bullet+}$ radical cation appeared[10e] at λ_{max} = 450 and 680 nm, while the $STTFS^{2+}$ dication absorption band was centered[10e] (Figure 2b) around 534 nm. In the case of **1**, after the addition of 2 equiv of $Fe(ClO_4)_3$, a peak centered on 780 nm appeared in addition to peaks around 400 and 560 nm (Figure 2c). The addition of oxidant until the fully oxidized state $\mathbf{1}^{4+}$ was reached resulted in sharp absorption bands corresponding to the $OTTFO^{2+}$ and $STTFS^{2+}$ dications at 386 and 540 nm, respectively.

According to previous studies,[13−16] the peak at 780 nm is indicative of intramolecular radical−radical interactions occurring within $\mathbf{1}^{2(\bullet+)}$. The fact that the absorption bands at 400 and 560 nm are blue-shifted compared to $OTTFO^{\bullet+}$ and $STTFS^{\bullet+}$ is also consistent with this hypothesis. These three bands appear after the addition of 1 equiv of $Fe(ClO_4)_3$, and their intensities reach a maximum after 2 equiv of $Fe(ClO_4)_3$ has been added. After the addition of 3 equiv of $Fe(ClO_4)_3$, two (400 and 780 nm) of these bands experience a decrease in intensity, and, after the addition of another 1 equiv of $Fe(ClO_4)_3$, which oxidizes **1** fully to generate the $OTTFO^{2+}$ and $STTFS^{2+}$ dications, all three bands disappear. The fact that the absorption bands that result after addition of 4 equiv of $Fe(ClO_4)_3$ are at the same wavelength as those of $OTTFO^{2+}$ and $STTFS^{2+}$ in **2** and **3**, respectively, indicates that these dicationic units are no longer dimerized—in all likelihood they are repelling each other as a result of Coulombic forces.

EPR experiments (Figure 3) were also performed in order to investigate the formation of the radical cation heterodimer in $\mathbf{1}^{2(\bullet+)}$. The EPR samples were prepared in a glovebox, ensuring the absence of O_2 and allowing us to resolve the hyperfine splittings of the $OTTFO^{\bullet+}$ and $STTFS^{\bullet+}$ radical cations. First of all, the EPR spectrum of **2**, after addition of 1 equiv of $Fe(ClO_4)_3$, possesses (Figure 3a) numerous hyperfine splittings superimposed on the spectral envelope, while in the case of the spectrum of **3**, after addition of 1 equiv of $Fe(ClO_4)_3$, the $STTFS^{\bullet+}$ radical cation displays (Figure 3b) only three hyperfine lines with 1.5 G spacing. The difference in the number of hyperfine lines in $OTTFO^{\bullet+}$, in comparison with those in $STTFS^{\bullet+}$, is a result of the methylene group which connects the oxygen atom to the TTF core in **2**. To be more specific, fewer protons interact with the $STTFS^{\bullet+}$ radical cation, since the sulfur atoms are connected directly to the TTF core.

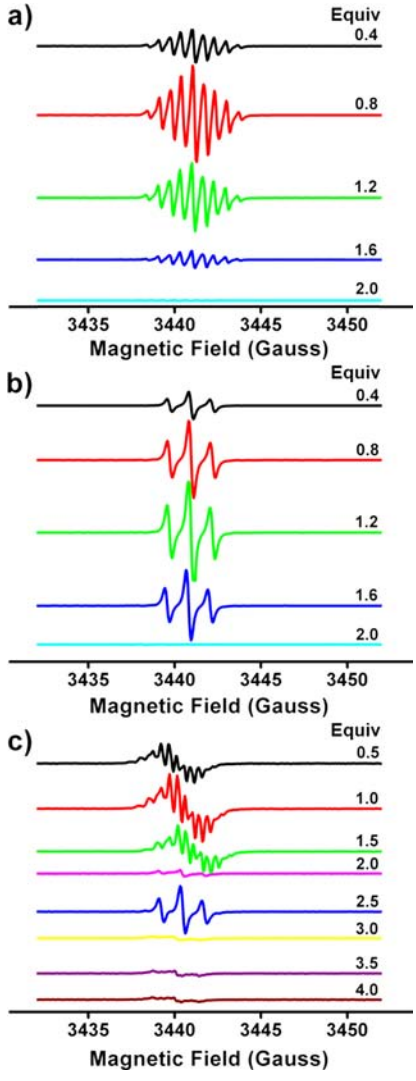

Figure 3. EPR spectra (MeCN, 298 K) of a 3.0×10^{-4} M solution of (a) OTTFO-TEG, (b) STTFS-TEG, and (c) macrocyclic polyether **1** after the addition of different equivalents (right) of $Fe(ClO_4)_3$.

dx.doi.org/10.1021/ja307577t | J. Am. Chem. Soc. 2012, 134, 19136−19145

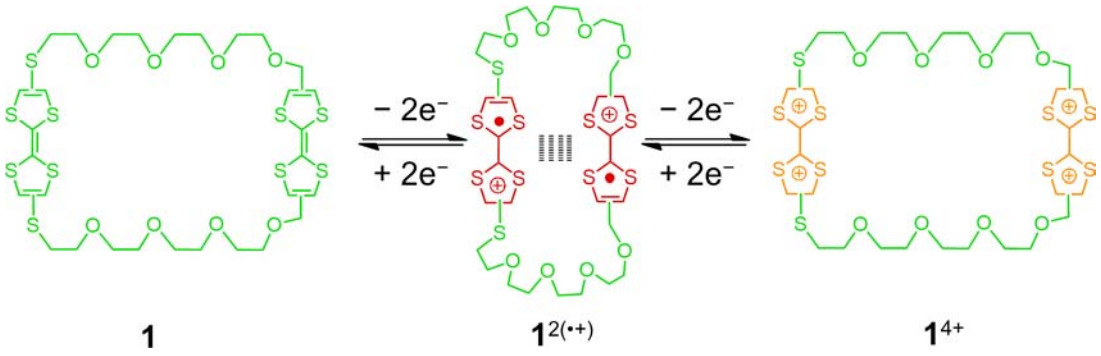

Figure 4. Simplified stepwise oxidative dimerization mechanism of the macrocyclic polyether **1**.

Scheme 2. Template-Directed Synthesis of the [2]Catenane 6·4PF$_6$, in Which the Macrocyclic Polyether 1 Acts as Template for Formation of the Mechanically Interlocked CBPQT^{4+} Ring

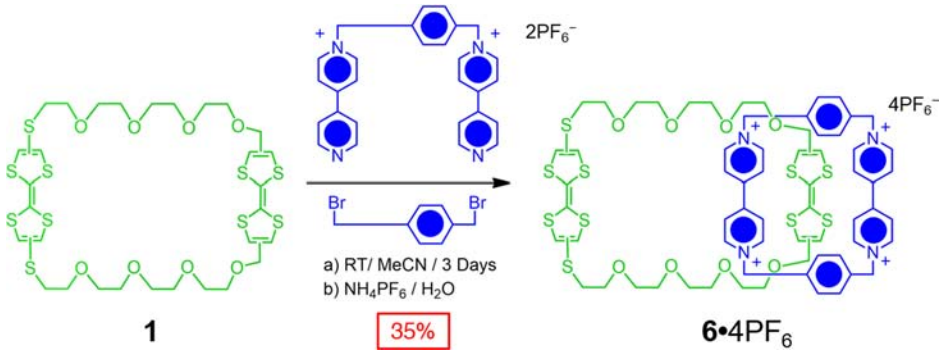

This difference allows us to distinguish signals arising from specifically either the OTTFO$^{\bullet+}$ or STTFS$^{\bullet+}$ units in the EPR spectra during the titration (Figure 3c) of **1** with Fe(ClO$_4$)$_3$. After 0.5 equiv of Fe(ClO$_4$)$_3$ has been added to the solution of **1**, the spectrum shows a hyperfine splitting pattern which matches the OTTFO$^{\bullet+}$ radical cation and reaches a maximum at 1 equiv of Fe(ClO$_4$)$_3$. The OTTFO$^{\bullet+}$ hyperfine splittings observed in **1** are slightly less well resolved, an observation which can be explained by the slower rotational correlation time of **1** compared to that of the smaller control compound **2**. Since the hyperfine splittings displayed in the spectrum of **1** after a one-electron oxidation match those of **2**$^{\bullet+}$, the radical electron is localized primarily on the OTTFO unit, and there is no strong evidence for the formation of a thermodynamically stable mixed-valence state. After 2 equiv of Fe(ClO$_4$)$_3$ has been added, the EPR signal tends to zero, suggesting that a strongly coupled (singlet) [OTTFO$^{\bullet+}$···STTFS$^{\bullet+}$] heterodimer has been formed in solution. Addition up to 4 equiv of Fe(ClO$_4$)$_3$ results in the formation of the completely oxidized species—containing OTTFO^{2+} and STTFS^{2+}—which bears no radical character and is also EPR silent.

In order to rationalize the oxidation events in **1**, we propose the partial mechanism shown in Figure 4. Since the first oxidation potential of OTTFO is lower than that of STTFS, a small amount of OTTFO$^{\bullet+}$ is present at equilibrium, a fact which is confirmed by EPR spectroscopy. The appearance of the bands—corresponding to the [OTTFO$^{\bullet+}$···STTFS$^{\bullet+}$] radical heterodimer after the addition of 1 equiv of Fe(ClO$_4$)$_3$ in the UV−vis spectrum—suggests that there is a fast equilibrium taking place between **1**, **1**$^{\bullet+}$, and **1**$^{2(\bullet+)}$, a suggestion supported by the fact that the first oxidation wave in the CV appears as a single two-electron process. Addition of up to 2 equiv of Fe(ClO$_4$)$_3$ results in the nearly quantitative formation of a [OTTFO$^{\bullet+}$···STTFS$^{\bullet+}$] radical heterodimer, as indicated by the loss of any EPR signal. In order for the OTTFO$^{\bullet+}$and STTFS$^{\bullet+}$ radical cations to interact and form the [OTTFO$^{\bullet+}$···STTFS$^{\bullet+}$] radical heterodimer, a van der Waals distance of about 3 Å between the two radical cations is required. Indeed, the flexibility of the glycol linkers, in combination with the preorganized geometry of the macrocyclic polyether **1**, facilitates the formation of the [OTTFO$^{\bullet+}$···STTFS$^{\bullet+}$] radical heterodimer.[22] The addition of up to 4 equiv of Fe(ClO$_4$)$_3$ results in the OTTFO^{2+} and STTFS^{2+} dications. We hypothesize[23] that on account of strong Coulombic repulsion, the OTTFO^{2+} and STTFS^{2+} distance themselves from each other.

Catenane 6·4PF$_6$. Tetracationic cyclophanes such as CBPQT^{4+} are an important class of π-electron-deficient receptors which exhibit[24] excellent binding affinities for π-electron-rich guests. By using donor−acceptor template-directed protocols, CBPQT^{4+} has been incorporated into mechanically interlocked molecules[25] (MIMs), which have attracted considerable attention and impacted areas in nanotechnology ranging from molecular electronic devices[11] to stimuli-responsive therapeutic materials.[26]

The macrocyclic polyether **1** has been used to template the formation of the CBPQT^{4+} ring component, producing the [2]catenane **6**·4PF$_6$ whereby a clipping strategy was used to form the mechanical bond. The template-directed synthesis of the [2]catenane **6**·4PF$_6$ in 35% yield starting from **1** is shown in Scheme 2. There are two co-conformations of the [2]catenane **6**·4PF$_6$—one in which the CBPQT^{4+} ring encircles the OTTFO unit and the other one in which the CBPQT^{4+} ring encircles the STTFS unit. Since OTTFO-TEG binds more strongly with CBPQT^{4+} than does STTFS-TEG in a host−guest context—K_a = 416 000[12c] and 8580 M^{-1},[10e] respec-

dx.doi.org/10.1021/ja307577t | J. Am. Chem. Soc. 2012, 134, 19136−19145

tively—we hypothesize that in 6^{4+} the $CBPQT^{4+}$ ring encircles the OTTFO unit primarily, an assertion which has been corroborated by UV–vis spectroscopy.

Slow vapor diffusion of $^{i}Pr_2O$ into an MeCN solution of $6{\cdot}4PF_6$ at room temperature afforded[27] green crystals suitable for X-ray crystallography. The solid-state structure of $6{\cdot}4PF_6$ is illustrated in Figure 5. The OTTFO unit is encircled exclusively

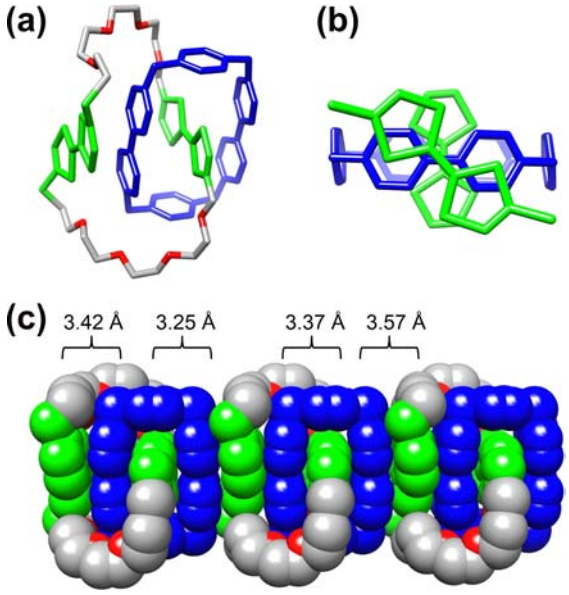

Figure 5. Solid-state structure of $6{\cdot}4PF_6$ obtained by single-crystal X-ray crystallography: (a) Wire-fame representation of 6^{4+}. (b) Side-on perspective of 6^{4+}. (c) Space-filling representation of the long-range packing of the catenanes. The counterions, hydrogen atoms, and disordered solvent molecules are omitted for the sake of clarity. The $CBPQT^{4+}$ ring is shown in blue, the TTF units in green, the sulfur in green, the oxygens in red, and the carbons of the macrocyclic polyether in gray.

by the $CBPQT^{4+}$ ring in preference to the STTFS unit. The interplanar separations between the OTTFO unit with the outside and inside bipyridinium ($BIPY^{2+}$) units of the $CBPQT^{4+}$ ring are 3.25 and 3.37 Å, respectively, while the plane-to-plane distance between the STTFS unit and the inside $BIPY^{2+}$ is 3.42 Å. The solid-state superstructure of $6{\cdot}4PF_6$ is mediated by noncovalent donor–acceptor [$\pi\cdots\pi$] interactions between the STTFS unit and the $CBPQT^{4+}$ rings, resulting in an infinite donor–acceptor stack: the distance between the STTFS unit and the $BIPY^{2+}$ units of an adjacent catenane is 3.57 Å. Both the OTTFO and STTFS units adopt *trans* configurations in the solid state, presumably in order to maintain geometries favorable for [C–H···O] interactions—between the glycol oxygens and the hydrogens α to the pyridinium nitrogens—which are known[24c] to stabilize $CBPQT^{4+}$-based host–guest complexes.

The CV of the catenane 6^{4+} reveals (Figure 6) two reversible redox processes occurring at potentials of +0.51 and +0.80 V. In order to determine quantitatively the number of electrons corresponding to each process, we appealed to chronocoulometry (CC) and the Anson equation,

$$Q = 2nFACD^{1/2}\pi^{-1/2}t^{1/2} \quad (1)$$

where Q is the amount of charge transferred, n is the number of electrons transferred per molecule, F is Faraday's constant, A is the electrode area, D is the diffusion coefficient, and C is concentration. A linear relationship exists between Q and $t^{1/2}$, allowing us to determine the value of n. We made the assumption that the diffusion coefficient of the catenane undergoes only minor changes as a function of oxidation state. The number of electrons transferred per molecule can then be determined by the ratio of the slopes of the Anson plot. First, the potential was set from 0 to +0.63 V, and the amount of charge passed was monitored as a function of time. An Anson plot revealed a slope of 19.4 $\mu Q\ s^{-1/2}$. Next, the potential was set from 0 to +1.0 V—enough to access both redox processes—and the corresponding Anson plot revealed a slope of 77.8 $\mu Q\ s^{-1/2}$. By applying the Anson equation, the ratio of the number of electrons transferred in the second process with respect to the first one is 4.01. It follows that the first redox event is a one-electron process, while the second one is a three-electron process.

The redox-activated switching processes of the catenane $6{\cdot}4PF_6$ were studied more extensively by UV–vis spectroscopy. Initially, a CT band corresponding to encirclement of the OTTFO unit by the $CBPQT^{4+}$ ring (λ_{max} = 850 nm) can be observed. The symmetric nature of the band suggests that the ground-state distribution of translational isomers is a >10:1 ratio in favor of encirclement of the OTTFO units by $CBPQT^{4+}$ rings. If the ground-state distribution of translational isomers were to lie more in favor of encirclement of the STTFS unit, a band would be observed[10e] at 800 nm. After addition of 1 equiv of $Fe(ClO_4)_3$ to 6^{4+}, the intensity of the CT band at 850 nm decreased (Figure 7). Meanwhile, two new bands centered on 450 and 610 nm, as well as a broad peak centered

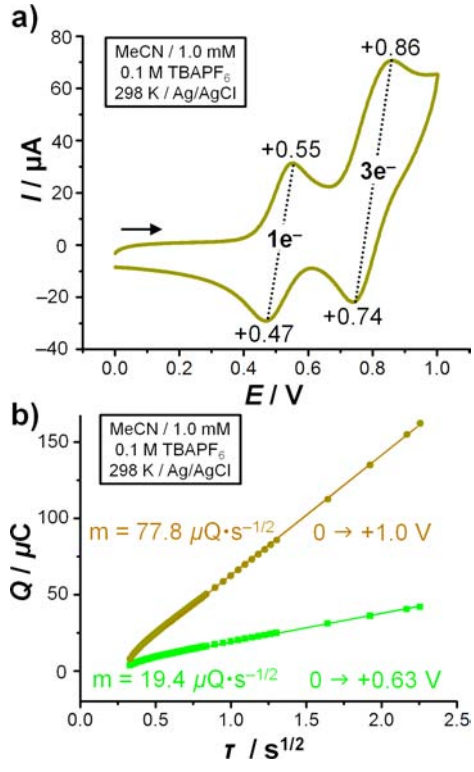

Figure 6. (a) CV of $6{\cdot}4PF_6$ recorded at a scan rate of 500 mV s^{-1}. (b) Anson plot of the CC experiments performed on the catenane under identical conditions. The ratio of the slopes of the best-fit lines indicates that the first redox process is a one-electron and the second a three-electron one.

dx.doi.org/10.1021/ja307577t | J. Am. Chem. Soc. 2012, 134, 19136–19145

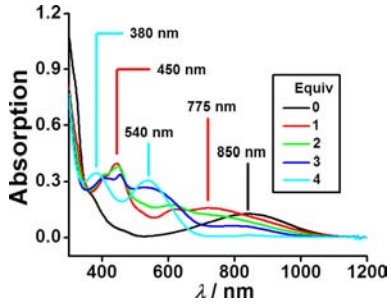

Figure 7. UV−vis absorption spectra (MeCN, 298 K) of a 1.0×10^{-4} M solution of **6**·4PF_6 and of the same solution after addition of 1.0, 2.0, 3.0, and 4.0 equiv of $Fe(ClO_4)_3$.

around 775 nm, appeared. In the knowledge that TTF derivatives encircled by the $CBPQT^{4+}$ ring are significantly more difficult to oxidize, initially we expected that the outside STTFS unit would be the thermodynamically oxidized product. The band appearing at 610 nm in the UV−vis spectrum, however, supports the views that an appreciable amount of $OTTFO^{\bullet+}$ is generated, despite the fact that it is encircled preferentially by the $CBPQT^{4+}$ ring in the ground state, an observation which indicates that a more complicated mechanism of oxidation is at play. Further addition of up to 2 equiv of $Fe(ClO_4)_3$ does not result in a sharp band centered around 780 nm, an observation which suggests no radical dimer is formed, most likely because of the steric hindrance provided by the $CBPQT^{4+}$ ring. There is still, however, a broad band observed between 700 and 1050 nm, which may be attributed to the electronic interaction between $OTTFO^{\bullet+}$ and $STTFS^{\bullet+}$. After the addition of 4 equiv of $Fe(ClO_4)_3$ to the solution of **6**·4PF_6, sharp absorption bands at 380 and 540 nm—corresponding to the fully oxidized $OTTFO^{2+}$ and $STTFS^{2+}$ units, respectively—are observed, most likely indicating that the dications are repelled Coulombically from each other as well as from the $CBPQT^{4+}$ ring.

Next, we appealed to EPR spectroscopy in order to gain further insight into the mechanism of switching in **6**·4PF_6. All the EPR spectra of the [2]catenane were recorded (Figure 8) in MeCN (0.2 mM) at room temperature. After addition of 1 equiv of $Fe(ClO_4)_3$ to generate the singly oxidized state, the spectrum shows EPR signals arising from both $OTTFO^{\bullet+}$ and $STTFS^{\bullet+}$. This spectrum can be reconstructed from the EPR spectra of $\mathbf{2}^{\bullet+}$ and $\mathbf{3}^{\bullet+}$ (Figures S2−S4). In particular, the EPR spectrum fits well with a linear combination of the separate $\mathbf{2}^{\bullet+}$ and $\mathbf{3}^{\bullet+}$ spectra, indicating that the $OTTFO^{\bullet+}$ and $STTFS^{\bullet+}$ do not interact when the macrocyclic polyether is catenated by a $CBPQT^{4+}$ ring. From the curve fitting, we have calculated that the ratio of $OTTFO^{\bullet+}$ and $STTFS^{\bullet+}$ in the solution approaches approximately 70:30 after a total of 1 equiv of the oxidant is reached (Table 1). Despite the fact that the oxidation potential

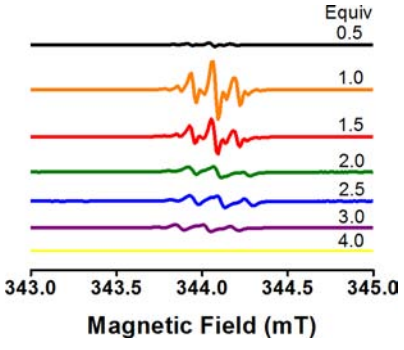

Figure 8. EPR spectra (MeCN, 298 K) of a 2.0×10^{-4} M solution of **6**·4PF_6 after addition of different amounts of $Fe(ClO_4)_3$. The spectra for 2−4 equiv of oxidant are magnified by a factor of 2 for the sake of clarity.

Table 1. Summary of the Ratios of $OTTFO^{\bullet+}$ and $STTFS^{\bullet+}$ and the Rate of Interaction between the $OTTFO^{\bullet+}$ and $STTFS^{\bullet+}$ As Obtained from Simulations of the Titration-Dependent Spectra Shown in Figure 8

molar equiv of $Fe(ClO_4)_3$	% contribution from $OTTFO^{\bullet+}$	% contribution from $STTFS^{\bullet+}$	additional line width[a] in spectrum (G)	k (s^{-1} M^{-1})
0.25	60	40	<0.01	$<2.3 \times 10^9$
0.50	67	33	<0.01	$<1.2 \times 10^9$
0.75	71	29	0.01	8.6×10^8
1.00	71	29	0.03	1.6×10^9
1.25	70	30	0.13	6.0×10^9
1.50	77	23	0.20	7.8×10^9
1.75	69	31	0.26	8.6×10^9
2.00	64	36	0.28	8.1×10^9
2.25	68	32	0.32	9.3×10^9
2.50	71	29	0.26	7.6×10^9
2.75	71	29	0.23	6.9×10^9
3	71	29	0.24	7.0×10^9

[a]"Additional line width" is the broadening in the spectrum caused by the exchange interaction.

of the encircled OTTFO unit is much greater than that of the free STTFS unit, after a one-electron oxidation, the thermodynamic equilibrium involves an interplay between translational and electronic isomers, and the OTTFO units are oxidized more readily than the STTFS units.

After addition of more than 1 equiv of $Fe(ClO_4)_3$, as well as noting the presence of both $OTTFO^{\bullet+}$ and $STTFS^{\bullet+}$, there is a broadening of the spectra. Since the EPR spectra of $OTTFO^{\bullet+}$ and $STTFS^{\bullet+}$ do not exhibit broadening at this concentration (0.2 mM), the EPR spectra of **6**·4PF_6, after addition of more than of 1 equiv of $Fe(ClO_4)_3$, could not be simulated by a simple linear combination of $OTTFO^{\bullet+}$ and $STTFS^{\bullet+}$ spectra. Electron spin exchange between two radicals in solution is known to give rise to an additional Lorentzian line width[28] in the EPR spectra. This feature is consistent qualitatively with both the broadened EPR spectra and the appearance of the broad band between 700 and 1050 nm in the UV−vis spectrum. We assume that the spin exchange is most likely occurring between $OTTFO^{\bullet+}$ and $STTFS^{\bullet+}$, which means the $OTTFO^{\bullet+}$ and $STTFS^{\bullet+}$ units experience long-range interactions with each other, even in the presence of the $CBPQT^{4+}$ ring. In order to simulate the effect of spin exchange, the $OTTFO^{\bullet+}$ and $STTFS^{\bullet+}$ spectra were convoluted with the Lorentzian function and matched with the experimental spectra by using the relative proportions of $OTTFO^{\bullet+}$ and $STTFS^{\bullet+}$ and the line width of the Lorentzian as fitting parameters. It is clear that from 1.5 to 3 equiv of oxidant added, the ratio of $OTTFO^{\bullet+}$ to $STTFS^{\bullet+}$ remains 70:30 (Table 1), and the exchange interaction rate is on the order of $(7-9) \times 10^9$ s^{-1} M^{-1}. Since the exchange interaction is intramolecular and not intermolecular, we hypothesize that this spin exchange rate can be explained by the rate of translational motion of the $CBPQT^{4+}$ ring around the macrocyclic polyether. When the

dx.doi.org/10.1021/ja307577t | J. Am. Chem. Soc. 2012, 134, 19136−19145

CBPQT^{4+} ring is displaced from a neutral TTF unit by thermal energy, an intramolecular spin exchange may occur between the singly oxidized and unoxidized TTF units. This equilibrium process occurs upon the addition of even 0.25 equiv of oxidant and results in a rate of motion which is independent of the amount of further oxidant added: this situation is reflected in the relatively constant motional rates calculated.

From the EPR and electrochemistry experiments, we can deduce a switching mechanism (Figure 9) which governs the redox behavior of the [2]catenane **6**·4PF$_6$. In the initial state of the catenane, OTTFO is encircled by the CBPQT^{4+} ring. After the first one-electron wave at +0.55 V, the approximate 70:30 ratio of electronic translational isomers is established. As a consequence of fast equilibration of the redox-stimulated translational motion of the CBPQT^{4+} ring, only a single one-electron redox process is observed. This one-electron redox process is assigned to the oxidation of both the OTTFO and STTFS units, in the 70:30 ratio measured from EPR. The next oxidation process—a three-electron one—directly converts the +1 oxidation state to the +4 state, an observation which indicates that the +2 and +3 states are not thermodynamically stable intermediates. The CBPQT^{4+} ring acts to stabilize the +1 oxidation state of the macrocyclic polyether component while disrupting the stability of the +2 oxidation state, presumably by interfering with the favorable intramolecular radical–radical interactions between the two TTF units that are observed in the case of the free macrocyclic polyether **1**.

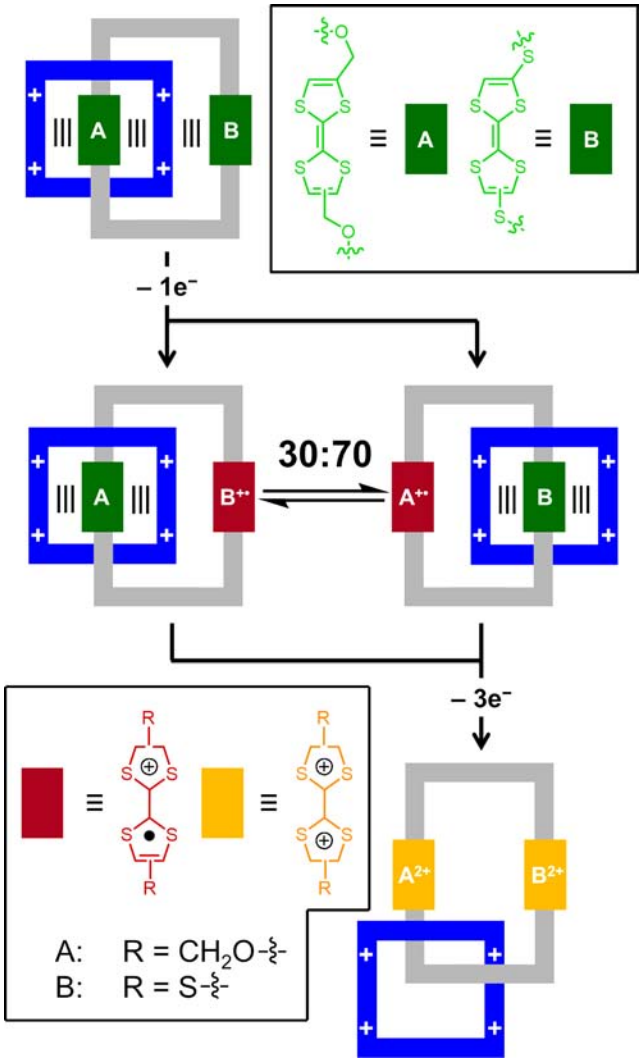

Figure 9. Proposed stepwise oxidation mechanism of **6**·4PF$_6$. After the first one-electron process, a thermodynamic equilibrium is established in which the ratio of OTTFO$^{\bullet+}$ to STTFS$^{\bullet+}$, and thus the ratio of translational isomers, is 70:30. Further oxidation occurs as a three-electron process, resulting in the fully oxidized species.

CONCLUSION

In summary, the stabilization of TTF radical cation dimers between TTF units of different constitutions has been demonstrated. Although individually the radical cation states of OTTFO and STTFS units exhibit different electrochemical and spectroscopic properties, when preorganized covalently within a macrocyclic polyether, the OTTFO$^{\bullet+}$ and STTFS$^{\bullet+}$ units still form stabilized radical cation dimers. In a [2]catenane in which the macrocyclic polyether is interlocked mechanically with a CBPQT^{4+} ring, the existence of the ring prevents sterically, if not also electrostatically, the formation of radical cation dimers, yet the OTTFO$^{\bullet+}$ and STTFS$^{\bullet+}$ radical cations still experience long-range spin exchange interactions with each other. These findings provide a fundamental understanding of the mechanism of radical cation dimer formation, not just between identical TTF units but also between TTF units of different constitutions, and could also contribute in time to the development of TTF-based molecular electronic devices in which specific redox tuning can be achieved by utilizing a mixture of constitutionally different TTF derivatives.

EXPERIMENTAL SECTION

General Methods. All reagents and starting materials were purchased from Aldrich or VWR and used without further purification. All reactions were performed under an argon atmosphere and in dry solvents unless otherwise noted. UV–vis spectra were recorded with a Shimadzu TU-1800pc UV–vis spectrophotometer at 298 K. NMR spectra were recorded on Bruker Avance-500 at 500 MHz spectrometers at ambient temperature. Deuterated solvents (Cambridge Isotope Laboratories) for NMR spectroscopic analyses were used as received. All chemical shifts are quoted in ppm relative to the signals corresponding to the residual non-deuterated solvents ($CDCl_3$, 7.26 ppm; CD_3CN, 1.94 ppm). High-resolution electrospray ionization (HR ESI) mass spectra were measured on Agilent 6210 LC-TOF with Agilent 1200 HPLC introduction. High-resolution matrix-assisted laser desorption/ionization (MALDI) mass spectra were measured on a Bruker Autoflex III mass spectrometer. Electrochemical experiments were carried out at 298 K in argon-purged MeCN solutions, with a Gamry Reference 600 potentiostat interfaced to a PC. The working electrode was a glassy carbon (0.071 cm^2) and its surface was polished routinely with 0.05 μm alumina-water slurry on a felt pad immediately before use. The counter electrode was a Pt coil and the reference electrode was a standard Ag/AgCl electrode. The concentration of the sample and supporting electrolyte (NBu_4PF_6) were 0.5×10^{-3} mol L^{-1} and 0.1 mol L^{-1}, respectively. EPR measurements at X-band (9.5 GHz) were carried out at room temperature using a Bruker Elexsys E580-X EPR spectrometer outfitted with a variable Q dielectric resonator (ER-4118X-MD5-W1). All the samples were dissolved in degassed MeCN and prepared in a N_2-filled glovebox to ensure the absence of oxygen. All measurements were made on a Bruker APEX-II CCD with graphite-monochromated Cu Kα radiation. Intensities were corrected for Lorentz polarization and for absorption. The structures were solved by direct methods. Hydrogen atoms bound to carbon were idealized. Structural refinements were obtained with full-matrix least-squares based on F^2 by using the program SHELXTL.

dx.doi.org/10.1021/ja307577t | J. Am. Chem. Soc. 2012, 134, 19136–19145

Synthesis. Compound **2** (OTTFO-TEG),[19] compound **3** (STTFS-TEG),[10e,29] 4,4′,(5′)-bis(2-cyanoethylthio)tetrathiafulvalene[20] **5**, and 1,1′-[1,4-phenylenebis(methylene)]-bis(4,4′-bipyridinium) bis(hexafluorophospate)[30] were prepared following literature procedures.

1. A solution of **4** (0.92 g, 1.0 mmol) and **5** (0.37 g, 1.0 mmol) in anhydrous degassed THF (50 mL) was added very slowly to a solution of $CsOH·H_2O$ (0.67 g, 4 mmol) in anhydrous degassed THF (140 mL) and MeOH (20 mL) during 20 h at room temperature. After finishing the addition, the reaction was stirred for 4 h, after which the solvents were evaporated under reduced pressure, and the resulting residue was subjected to column chromatography [SiO_2:EtOAc/CH_2Cl_2 (1:2)]. The product **1** was isolated as yellow oil (0.26 g, yield, 31%). ^{1}H NMR ($CDCl_3$, 500 MHz, 298 K): δ (ppm) = 6.43−6.41 (m, 2H), 6.23−6.21 (m, 2H), 4.28 (m, 4H), 3.68−3.60 (m, 28H), 2.94−2.90 (m, 4H). ^{13}C NMR ($CDCl_3$, 125 MHz, 298 K, ppm): δ = 134.7, 134.6, 134.5, 126.6, 126.5, 126.4, 123.3, 123.1, 123.0, 116.5, 116.4, 112.5, 112.3, 112.3, 112.2, 110.7, 110.7, 70.8, 70.7, 70.7, 70.7, 70.6, 70.6, 69.8, 69.7, 69.6, 69.6, 69.3, 69.3, 69.3, 69.2, 68.3, 35.3, 35.2, 35.1. HR MS (ESI): calcd for $C_{30}H_{40}O_8S_{10}$ m/z = 847.9925 $[M]^{\bullet+}$, 423.9960 $[M]^{2+}$, found m/z = 847.9925 $[M]^{\bullet+}$, 423.9958 $[M]^{2+}$.

4. Et_3N (1.09 g, 1.50 mL, 10.7 mmol) and *N*,*N*′-dimethylaminopyridine (DMAP) (50 mg) were added to a solution of **2** (985 mg, 1.60 mmol) in dry CH_2Cl_2 (50 mL) at 0 °C under a N_2 atmosphere. A solution of *p*-toluene-sulfonyl chloride (0.92 g, 4.8 mmol) in dry CH_2Cl_2 (20 mL) was added directly to the reaction over 1 h. The reaction mixture was allowed to warm up to room temperature before being stirred for an additional 11 h. After removal of the solvents under reduced pressure, the resulting mixture was purified by column chromatography [SiO_2:CH_2Cl_2/MeOH (100:1)]. The product ditosylate **4** was isolated as a yellow oil (1.08 g, yield, 72%). ^{1}H NMR ($CDCl_3$, 500 MHz, 298 K): δ (ppm) = 7.78 (d, J = 8.5 Hz, 4H), 7.33 (d, J = 8.5 Hz, 4H), 6.21 (s, 2H), 4.27 (s, 4H), 4.14 (t, J = 4.5 Hz, 4H), 3.68−3.58 (m, 28H), 2.44 (s, 6H). ^{13}C NMR ($CDCl_3$, 125 MHz, 298K, ppm): δ = 144.9, 134.5, 134.5, 132.9, 129.9, 128.0, 116.5, 116.3, 110.6, 110.5, 70.8, 70.6, 70.6, 70.6, 70.5, 69.3, 69.2, 68.7, 68.2, 68.2, 21.7. MALDI−TOF MS: calcd for $C_{38}H_{52}O_{14}S_6$ m/z = 924.168 $[M]^+$, found m/z = 924.164 $[M]^+$.

6·4PF$_6$. A mixture of 1,4-bis(bromomethyl)benzene (105 mg, 0.40 mmol), 1,1′-[1,4-phenylenebis(methylene)]-bis(4,4′-bipyridinium) bis(hexafluorophospate) (285 mg, 0.40 mmol) and the macrocyclic polyether **1** (85 mg, 0.10 mmol) was dissolved in MeCN (20 mL). The reaction mixture was stirred at room temperature for 3 days, and the resulting green solution was subjected to column chromatography [SiO_2:Me_2CO/NH_4PF_6 (100:1, v/w)]. The green band was collected. Most of the solvent was removed under reduced pressure, followed by addition of H_2O (30 mL). The precipitate was collected by filtration and washed with H_2O (3 × 20 mL) to give the pure product **6**·4PF_6 as a green solid (68 mg, 35%). Mp: ∼110 °C dec. ^{1}H NMR (CD_3CN, 500 MHz, 298 K): δ (ppm) = 9.11 (s, 4H), 9.00 (s, 4H), 7.89 (s, 4H), 7.79 (s, 4H), 7.70 (s, 8H), 6.51−6.42 (m, 2H), 6.24 (s, 2H), 5.78−5.70 (m, 8H), 4.18 (s, 4H), 3.96−3.40 (m, 28H), 2.94−2.84 (m, 4H). ^{13}C NMR (CD_3CN, 125 MHz, 298 K, ppm): δ = 146.2, 145.8, 145.6, 145.4, 144.8, 136.8, 133.7, 133.6, 131.8, 127.8, 127.7, 127.5, 126.6, 126.4, 126.2, 126.1, 122.4, 121.8, 120.3, 120.3, 108.9, 71.8, 71.7, 71.5, 71.4, 71.3, 70.9, 70.8, 70.8, 70.8, 70.7, 70.7, 70.5, 70.3, 70.1, 68.6, 65.5, 36.5, 36.3, 35.9. HR MS (ESI): calcd for $C_{66}H_{72}F^{2+}$ m/z = 504.4061 $[M - PF_6]^{3+}$, found m/z = 829.0923 $[M - 2PF_6]^{2+}$, 504.4066 $[M - PF_6]^{3+}$.

■ ASSOCIATED CONTENT

Ⓢ Supporting Information

EPR investigations and crystallographic information. This material is available free of charge via the Internet at http://pubs.acs.org.

■ AUTHOR INFORMATION

Corresponding Author

m-wasielewski@northwestern.edu; stoddart@northwestern.edu

Notes

The authors declare no competing financial interest.

■ ACKNOWLEDGMENTS

The research was sponsored by the Air Force Office of Scientific Research (AFSOR) under the Multidisciplinary Research Program of the University Research Initiative (MURI) award no. FA9550-07-1-0534 on "Bioinspired Supramolecular Enzymatic Systems" and the National Science Foundation (NSF) under the auspices of award no. CHE-0924620. D.C. and A.C.F. acknowledge the NSF for Graduate Research Fellowships. D.C., A.C.F., and J.F.S. were all beneficiaries of the WCU Program (NRF R-31-2008-000-10055-0) funded by the Ministry of Education, Science and Technology, Korea. M.R.W. acknowledges support by the NSF under grant CHE-1012378. M.T.C. thanks the Link Foundation for a fellowship. R.C. was supported as part of the ANSER Center, an Energy Frontier Research Center funded by the U.S. Department of Energy (DOE), Office of Science, Office of Basic Energy Sciences, under award no. DE-SC0001059.

■ REFERENCES

(1) (a) Friend, R. H.; Gymer, R. W.; Holmes, A. B.; Burroughes, J. H.; Marks, R. N.; Taliani, C.; Bradley, D. D. C.; Santos, D. A. D.; Brédas, J. L.; Logdlund, M.; Salaneck, W. R. *Nature* **1999**, *397*, 121−128. (b) MacDiarmid, A. G. *Angew. Chem., Int. Ed.* **2001**, *40*, 2581−2590. (c) Janata, J.; Josowicz, M. *Nat. Mater.* **2003**, *2*, 19−24. (d) Forrest, S. R. *Nature* **2004**, *428*, 911−918. (e) Heinze, J.; Frontana-Uribe, B. A.; Ludwigs, S. *Chem. Rev.* **2010**, *110*, 4724−4771.

(2) (a) Burroughes, J. H.; Bradley, D. D. C.; Brown, A. R.; Marks, R. N.; Mackay, K.; Friend, R. H.; Burns, P. L.; Holmes, A. B. *Nature* **1990**, *347*, 539−541. (b) Gross, M.; Muller, D. C.; Nothofer, H.-G.; Scherf, U.; Neher, D.; Brauchle, C.; Meerholz, K. *Nature* **2000**, *405*, 661−665. (c) Sandee, A. J.; Williams, C. K.; Evans, N. R.; Davies, J. E.; Boothby, C. E.; Köhler, A.; Friend, R. H.; Holmes, A. B. *J. Am. Chem. Soc.* **2004**, *126*, 7041−7048. (d) Perepichka, I. F.; Perepichka, D. F.; Meng, H.; Wudl, F. *Adv. Mater.* **2005**, *17*, 2281−2305.

(3) (a) Christoph, J, B. *Sol. Energ. Mat. Sol. C* **2004**, *83*, 273−292. (b) Guenes, S.; Neugebauer, H.; Sariciftci, N. S. *Chem. Rev.* **2007**, *107*, 1324−1338. (c) Kim, J. Y.; Lee, K.; Coates, N. E.; Moses, D.; Nguyen, T.-Q.; Dante, M.; Heeger, A. J. *Science* **2007**, *317*, 222−225.

(4) (a) Baumgarten, M.; Müllen, K. *Top. Curr. Chem.* **1994**, *169*, 1−103. (b) Miller, L. L.; Mann, K. R. *Acc. Chem. Res.* **1996**, *29*, 417−423. (c) Nishinaga, T.; Komatsu, K. *Org. Biomol. Chem.* **2005**, *3*, 561−569.

(5) (a) *Electronic Materials: The Oligomer Approach*; Müllen, K., Wegner, G., Eds.; Wiley: Weinheim, 1998. (b) Zade, S. S.; Zamoshchik, N.; Bendikov, M. *Acc. Chem. Res.* **2011**, *44*, 14−24.

(6) (a) Hill, M. G.; Mann, K. R.; Miller, L. L.; Penneau, J. F. *J. Am. Chem. Soc.* **1992**, *114*, 2728−2730. (b) Graf, D. D.; Campbell, J. P.; Miller, L. L.; Mann, K. R. *J. Am. Chem. Soc.* **1996**, *118*, 5480−5481. (c) Graf, D. D.; Duan, R. G.; Campbell, J. P.; Miller, L. L.; Mann, K. R. *J. Am. Chem. Soc.* **1997**, *119*, 5888−5899. (d) Zade, S. S.; Bendikov, M. *J. Phys. Chem. C* **2007**, *111*, 10662−10672.

(7) (a) Schafer, D. E.; Wudl, F.; Thomas, G. A.; Ferraris, J. P.; Cowan, D. O. *Solid State Commun.* **1974**, *14*, 347−351. (b) Yamada, J.; Sugimoto, T. *TTF Chemistry: Fundamentals and Applications of Tetrathiafulvalene*; Springer: Berlin, 2004.

(8) (a) Bryce, M. R. *J. Mater. Chem.* **2000**, *10*, 589−598. (b) Nielsen, M. B.; Lomholt, C.; Becher, J. *Chem. Soc. Rev.* **2000**, *29*, 153−164. (c) Jeppesen, J. O.; Nielsen, M. B.; Becher, J. *Chem. Rev.* **2004**, *104*, 5115−5131. (d) Segura, J. L.; Martín, N. *Angew. Chem., Int. Ed.* **2001**, *40*, 1372−1409. (e) Inagi, S.; Naka, K.; Chujo, Y. *J. Mater. Chem.* **2007**, *17*, 4122−4135. (f) Martin, N.; Sanchez, L.; Herranz, M. A.; Illescas,

B.; Guldi, D. M. *Acc. Chem. Res.* **2007**, *40*, 1015−1024. (g) Canevet, D.; Salle, M.; Zhang, G. X.; Zhang, D. Q.; Zhu, D. B. *Chem. Commun.* **2009**, 2245−2269. (h) Lorcy, D.; Bellec, N.; Fourmigué, M.; Avarvari, N. *Coord. Chem. Rev.* **2009**, *253*, 1398−1438.

(9) (a) Balzani, V.; Becher, J.; Credi, A.; Fyfe, M. C. T.; Mattersteig, G.; Menzer, S.; Nielsen, M. B.; Raymo, F. M.; Stoddart, J. F.; Venturi, M.; Williams, D. J. *J. Am. Chem. Soc.* **1999**, *121*, 3951−3957. (b) Jeppesen, J. O.; Becher, J. *Eur. J. Org. Chem.* **2003**, 3245−3266. (c) Zhao, Y.-L.; Aprahamian, I.; Trabolsi, A.; Erina, N.; Stoddart, J. F. *J. Am. Chem. Soc.* **2008**, *130*, 6348−6350. (d) Wang, C.; Chen, Q.; Sun, F.; Zhang, D.; Zhang, G.; Huang, Y.; Zhao, R.; Zhu, D. *J. Am. Chem. Soc.* **2008**, *132*, 3092−3096.

(10) (a) Li, Z.-T.; Stein, P. C.; Becher, J.; Jensen, D.; Mørk, P.; Svenstrup, N. *Chem. Eur. J.* **1996**, *2*, 624−633. (b) Asakawa, M.; Ashton, P. R.; Balzani, V.; Credi, A.; Hamers, C.; Mattersteig, G.; Montalti, M.; Shipway, A. N.; Spencer, N.; Stoddart, J. F.; Tolley, M. S.; Venturi, M.; White, A. J. P.; Williams, D. J. *Angew. Chem., Int. Ed.* **1998**, *37*, 333−337. (c) Jeppesen, J. O.; Perkins, J.; Becher, J.; Stoddart, J. F. *Angew. Chem., Int. Ed.* **2001**, *40*, 1216−1221. (d) Olson, M. A.; Botros, Y. Y.; Stoddart, J. F. *Pure Appl. Chem.* **2010**, *82*, 1569−1574. (e) Wang, C.; Olson, M. A.; Fang, L.; Benítez, D.; Tkatchouk, E.; Basu, S.; Basuray, A. N.; Zhang, D.; Zhu, D.; Goddard, W. A.; Stoddart, J. F. *Proc. Natl. Acad. Sci. U.S.A.* **2010**, *107*, 13991−13996.

(11) (a) Collier, C. P.; Mattersteig, G.; Wong, E. W.; Luo, Y.; Beverly, K.; Sampaio, J.; Raymo, F. M.; Stoddart, J. F.; Heath, J. R. *Science* **2000**, *289*, 1172−1175. (b) Flood, A. H.; Stoddart, J. F.; Steuerman, D. W.; Heath, J. R. *Science* **2004**, *306*, 2055−2056. (c) Heath, J. R.; Stoddart, J. F.; Williams, R. S. *Science* **2004**, *303*, 1136−1137. (d) Mas-Torrent, M.; Durkut, M.; Hadley, P.; Ribas, X.; Rovira, C. *J. Am. Chem. Soc.* **2004**, *126*, 984−985. (e) Mas-Torrent, M.; Rovira, C. *J. Mater. Chem.* **2006**, *16*, 433−436. (f) Green, J. E.; Choi, J. W.; Boukai, A.; Bunimovich, Y.; Johnston-Halperin, E.; DeIonno, E.; Luo, Y.; Sheriff, B. A.; Xu, K.; Shin, Y. S.; Tseng, H.-R.; Stoddart, J. F.; Heath, J. R. *Nature* **2007**, *445*, 414−417.

(12) (a) González, M.; Matín, N.; Segura, J.; Garín, J.; Orduna, J. *Tetrahedron Lett.* **1998**, *39*, 3269−3272. (b) Coronado, E.; Galan-Mascaros, J. R.; Gomez-Garcia, C. J.; Laukhin, V. *Nature* **2000**, *408*, 447−449. (c) Ikeda, T.; Saha, S.; Aprahamian, I.; Leung, K. C.-F.; Williams, A.; Deng, W.-Q.; Flood, A. H.; Goddard, W. A.; Stoddart, J. F. *Chem. Asian J.* **2007**, *2*, 76−93. (d) Fernández, G.; Sánchez, L.; Pérez, E. M.; Martín, N. *J. Am. Chem. Soc.* **2008**, *130*, 10674−10683. (e) Wenger, S.; Bouit, P.-A.; Chen, Q.; Teuscher, J.; Censo, D. D.; Humphry-Baker, R.; Moser, J.-E.; Delgado, J. L.; Martín, N.; Zakeeruddin, S. M.; Grätzel, M. *J. Am. Chem. Soc.* **2010**, *132*, 5164−5169.

(13) (a) Torrance, J. B.; Scott, B. A.; Welber, B.; Kaufman, F. B.; Seiden, P. E. *Phys. Rev. B* **1979**, *19*, 730−741. (b) Khodorkovsky, V.; Shapiro, L.; Krief, P.; Shames, A.; Mabon, G.; Gorgues, A.; Giffard, M. *Chem. Commun.* **2001**, 2736−2737. (c) Rosokha, S. V.; Kochi, J. K. *J. Am. Chem. Soc.* **2007**, *129*, 828−838. (d) Bejger, C.; Davis, C. M.; Park, J. S.; Lynch, V. M.; Love, J. B.; Sessler, J. L. *Org. Lett.* **2011**, *13*, 4902−4905. (e) Fahrenbach, A. C.; Barnes, J. C.; Lanfranchi, D. A.; Li, H.; Coskun, A.; Gassensmith, J. J.; Liu, Z.; Benítez, D.; Trabolsi, A.; Goddard, W. A.; Elhabiri, M.; Stoddart, J. F. *J. Am. Chem. Soc.* **2012**, *134*, 3061−3072.

(14) (a) Yakushi, K.; Nishimura, S.; Sugano, T.; Kuroda, H.; Ikemoto, I. *Acta Crystallogr. B* **1980**, *36*, 358−363. (b) Kathirgamanathan, P.; Mazi, M. A.; Rosseinsky, D. R. *J. Chem. Soc., Perkin Trans. 2* **1982**, 593−596. (c) Kondo, K.; Matsubayashi, G.; Tanaka, T.; Yoshioka, H.; Nakatsu, K. *J. Chem. Soc., Dalton Trans.* **1984**, 379−384. (d) Pyrka, G. J.; Fernando, Q.; Inoue, M. B.; Inoue, M. *Inorg. Chim. Acta* **1989**, *156*, 257−264. (e) Tanaka, K.; Kunita, T.; Ishiguro, F.; Naka, K.; Chujo, Y. *Langmuir* **2009**, *25*, 6929−6933.

(15) (a) Christensen, C. A.; Goldenberg, L. M.; Bryce, M. R.; Becher, J. *Chem. Commun.* **1998**, 509−510. (b) Spanggaard, H.; Prehn, J.; Nielsen, M. B.; Levillain, E.; Allain, M.; Becher, J. *J. Am. Chem. Soc.* **2000**, *122*, 9486−9494. (c) Lyskawa, J.; Sallé, M.; Balandier, J. Y.; Le Derf, F.; Levillain, E.; Allain, M.; Viel, P.; Palacin, S. *Chem. Commun.* **2006**, 2233−2235. (d) Aprahamian, I.; Olsen, J.-C.; Trabolsi, A.; Stoddart, J. F. *Chem. Eur. J.* **2008**, *14*, 3889−3895.

(16) (a) Ziganshina, A. Y.; Ko, Y. H.; Jeon, W. S.; Kim, K. *Chem. Commun.* **2004**, 806−807. (b) Yoshizawa, M.; Kumazawa, K.; Fujita, M. *J. Am. Chem. Soc.* **2005**, *127*, 13456−13457. (c) Chiang, P.-T.; Chen, N.-C.; Lai, C.-C.; Chiu, S.-H. *Chem. Eur. J.* **2008**, *14*, 6546−6552. (d) Saad, A.; Barriere, F.; Levillain, E.; Vanthuyne, N.; Jeannin, O.; Fourmigue, M. *Chem. Eur. J.* **2010**, *16*, 8020−8028.

(17) (a) Spruell, J. M.; et al. *Nature Chem.* **2011**, *2*, 870−879. (b) Barin, G.; Coskun, A.; Friedman, D. C.; Olson, M. A.; Colvin, M. T.; Carmielli, R.; Dey, S. K.; Bozdemir, O. A.; Wasielewski, M. R.; Stoddart, J. F. *Chem. Eur. J.* **2011**, *17*, 213−222. (c) Coskun, A.; Spruell, J. M.; Barin, G.; Fahrenbach, A. C.; Forgan, R. S.; Colvin, M. T.; Carmieli, R.; Benítez, D.; Tkatchouk, E.; Friedman, D. C.; Sarjeant, A. A.; Wasielewski, M. R.; Goddard, W. A.; Stoddart, J. F. *J. Am. Chem. Soc.* **2011**, *133*, 4538−4547.

(18) (a) Becher, J.; Lau, J.; Leriche, P.; Mork, P.; Svenstrup, N. *J. Chem. Soc., Chem. Commun.* **1994**, 2715−2716. (b) Garin, J.; Orduna, J.; Uriel, S.; Moore, A. J.; Bryce, M. R.; Wegener, S.; Yufit, D. S.; Howard, J. A. K. *Synthesis* **1994**, 489−493. (c) Moore, A. J.; Bryce, M. R. *Synthesis* **1997**, 407−409. (d) Simonsen, K. B.; Becher, J. *Synlett* **1997**, 1211−1220.

(19) Asakawa, M.; Ashton, P. R.; Balzani, V.; Credi, A.; Mattersteig, G.; Matthews, O. A.; Montalti, M.; Spencer, N.; Stoddart, J. F.; Venturi, M. *Chem. Eur. J.* **1997**, *3*, 1992−1996.

(20) Guo, X. F.; Zhang, D. Q.; Zhang, H. J.; Fan, Q. H.; Xu, W.; Ai, X. C.; Fan, L. Z.; Zhu, D. B. *Tetrahedron* **2003**, *59*, 4843−4850.

(21) (a) Bendikov, M.; Wudl, F.; Perepichka, D. F. *Chem. Rev.* **2004**, *104*, 4891−4945. (b) Han, C.-C.; Balakumar, R.; Thirumalai, D.; Chung, M.-T. *Org. Biol. Chem.* **2006**, *4*, 3511−3516.

(22) Unfortunately, attempts to grow crystals of the radical cation dimer $\mathbf{1}^{2(\bullet+)}$ suitable for X-ray crystallography have so far been unsuccessful.

(23) (a) Li, H.; Zhao, Y.-L.; Fahrenbach, A. C.; Kim, S.-Y.; Paxton, W. F.; Stoddart, J. F. *Org. Biomol. Chem.* **2011**, *9*, 2240−2250. (b) Hmadeh, M.; Fahrenbach, A. C.; Basu, S.; Trabolsi, A.; Benítez, D.; Li, H.; Albrecht-Gary, A.-M.; Elhabiri, M.; Stoddart, J. F. *Chem. Eur. J.* **2011**, *17*, 6076−6087.

(24) (a) Bernardo, A. R.; Stoddart, J. F.; Kaifer, A. E. *J. Am. Chem. Soc.* **1992**, *114*, 10624−10631. (b) Credi, V.; Balzani, S. J.; Langford, M.; Montalti, F. M.; Raymo; Stoddart, J. F. *New J. Chem.* **1998**, *22*, 1061−1065. (c) Sue, C. H.; Basu, S.; Fahrenbach, A. C.; Shveyd, A. K.; Dey, S. K.; Botros, Y. Y.; Stoddart, J. F. *Chem. Sci.* **2010**, *1*, 119−125.

(25) (a) Schill, G. *Catenanes, Rotaxanes, and Knots*; Academic Press: New York, 1971. (b) *Molecular Catenanes, Rotaxanes, and Knots*; Sauvage, J.-P., Dietrich-Buchecker, C., Eds.; Wiley-VCH: Weinheim, 1999. (c) Collin, J.-P.; Dietrich-Buchecker, C. P.; Gaviña, M. C.; Jimenez-Molero; Sauvage, J.-P. *Acc. Chem. Res.* **2001**, *34*, 477−487. (d) Stoddart, J. F.; Colquhoun, H. M. *Tetrahedron* **2008**, *64*, 8231−8263. (e) Stoddart, J. F. *Chem. Soc. Rev.* **2009**, *38*, 1802−1820. (f) Crowley, J. D.; Goldup, S. M.; Lee, A.-L.; Leigh, D. A.; McBurney, R. T. *Chem. Soc. Rev.* **2009**, *38*, 1530−1541. (g) Amabilino, D. B.; Pérez-García, L. *Chem. Soc. Rev.* **2009**, *38*, 1562−1571.

(26) (a) Angelos, S.; Johansson, E.; Stoddart, J. F.; Zink, J. I. *Adv. Funct. Mater.* **2007**, *17*, 2261−2271. (b) Cotí, K. K.; Belowich, M. E.; Liong, M.; Ambrogio, M. W.; Lau, Y. A.; Khatib, H. A.; Zink, J. I.; Khashab, N. M.; Stoddart, J. F. *Nanoscale* **2009**, *1*, 16−39. (c) Ambrogio, M. W.; Thomas, C. R.; Zhao, Y.-L.; Zink, J. I.; Stoddart, J. F. *Acc. Chem. Res.* **2011**, *44*, 903−913. (d) Li, Z.; Barnes, J. C.; Bosoy, A.; Stoddart, J. F.; Zink, J. I. *Chem. Soc. Rev.* **2012**, *41*, 2590−2605. (e) Wang, C.; Li, Z.; Cao, D; Zhao, Y.-L.; Gaines, J. W.; Bozdemir, O. A.; Ambrogio, M. W.; Frasconi, M.; Botros, Y. Y.; Zink, J. I.; Stoddart, J. F. *Angew. Chem., Int. Ed.* **2012**, *51*, 5460−5465.

(27) Crystal data for **6**•4PF_6: $C_{74}H_{84}F_{24}N_8O_8P_4S_{10}$, M_r = 2113.94, 0.45 × 0.42 × 0.17 mm, monoclinic, space group *C*2/*c*, *a* = 22.1794(18), *b* = 13.6101(10), and *c* = 29.949(2) Å, β = 96.671(5)°, *V* = 8979.4(12) Å^3, *Z* = 4, ρ_{calcd} = 1.564 g cm^{-3}.

(28) (a) Plachy, W.; Kivelson, D. *J. Chem. Phys.* **1967**, *47*, 3312−3318. (b) Eastman, M. P.; Kooser, R. G.; Das, M. R.; Freed, J. H. *J.*

Chem. Phys. **1969**, *51*, 2690−2709. (c) Weil, J. A.; Bolton, J. R. *Electron Paramagnetic Resonance: Elementary Theory and Practical Applications*, 2nd ed.; Wiley: Hoboken, NJ, 2007; pp 320−324.
(29) (a) Jia, C. Y; Zhang, D. Q.; Xu, W.; Zhu, D. B *Org. Lett.* **2001**, *3*, 1941−1944. (b) Jia, C. Y.; Zhang, D. Q.; Guo, X. F.; Wan, S. H.; Xu, W.; Zhu, D. B. *Synthesis* **2002**, *15*, 2177−2182.
(30) Ashton, P. R.; Huff, J.; Menzer, S.; Parsons, I. W.; Preece, J. A.; Stoddart, J. F.; Tolley, M. S.; White, A. J. P.; Williams, D. J. *Chem. Eur. J.* **1996**, *2*, 31−44.